Proceedings of the Twenty-sixth (2016) International Ocean and Polar Engineering Conference **www.isope.org**
Rhodes, Greece, June 26-July 1, 2016

ISBN 978-1-880653-88-3; ISSN 1098-6189

Numerical Simulation of Wind Effects on the Evolution of Freak Waves

Qing-Ping Zou and Hai-Fei Chen
Department of Civil and Environmental Engineering
University of Maine
Orono, Maine, USA

ABSTRACT

The wind effects on the evolution of a 2D dispersive focusing wave group are investigated using a two-phase flow model, which solves the Navier-Stokes equations for both air and water and captures the interface using the Volume of Fluid method. The turbulence is modeled by the standard Smagorinsky subgrid-scale stress model. The model predictions compare well with the experimental data without and with following wind action. Our model results show that the presence of following wind delays the wave group's focusing process and shifts the focus point downstream, while the presence of opposing wind slightly speeds up the focusing process and shifts the focus point upstream. The separate effects of wind-driven surface layer current on the wave group's evolution are examined. While both the depth-uniform and the strongly sheared drift current could cause the same shift of the focus point, the latter current leads to better agreement with the experimental data.

KEY WORDS: Freak wave; focusing wave group; two-phase flow; wind effect; drift current.

INTRODUCTION

Freak waves are extreme wave events focusing wave energy in a small area and during a short period of time. Freak waves seem not to have a single distinct cause, but occur where a number of physical factors such as strong winds and fast currents converge. As reviewed in Kharif and Pelinovsky (2003), the spatio-temporal focusing due to the dispersive nature of water waves is a classic formation mechanism for freak waves.

Touboul et al. (2006) and Kharif et al. (2008) studied experimentally the wind effects on freak waves, and concluded that the wind effects may shift the focusing point and increase the wave amplitude. The extreme wave events may also be sustained longer by the air flow separation occurring on the leeward side of the steep crests. Only qualitative agreements were, however, achieved in their numerical simulations. Tian and Choi (2013) investigated the wind effect on two-dimensional dispersive focusing wave groups and measured surface elevations under different wind speeds. These measurements serve as validation data to evaluate the present numerical model to address the wind-wave interaction problem.

Various numerical approaches have been developed to investigate the air flow and water wave interaction. Following Yan and Ma (2010), we divide them into one-phase and two-phase numerical models. In ocean wave fields predictions, the water waves are mostly simulated without directly considering the air flow (Chen et al., 2004; Touboul et al., 2006; Kharif et al., 2008; Yan and Ma, 2011; Tian and Choi, 2013; Liu et al., 2015). The wind effects are introduced through a free surface pressure model, which is typically based on Miles' shear flow instability theory (Miles, 1957) or Jeffreys' sheltering hypothesis (Jeffrey, 1925).

Two-phase numerical models, on the other hand, solve the Navier-Stokes equations for the air flow and water wave simultaneously in a fully coupled formulation (Fulgosi et al., 2003; Yan and Ma, 2010; Yang and Shen, 2011; Xie, 2014; Wen and Mobbs, 2014). To identify the air-water interface, either the air flow and water wave are solved in their respective domains so that the interface can be explicitly tracked, or both the air and water are solved in a single computational domain with the two phases considered as one fluid, and the interface is implicitly located by surface capturing methods like the Volume of Fluid (VOF) method (Hirt and Nichols, 1981), the level set method (Sethian, 2003; Wang et al., 2009; Zhang et al., 2010) or the Coupled Level Set and VOF method (Sussman and Puckett, 2000, Lv et al 2010)

Wind blows over the sea surface and exchanges momentum and energy with surface waves through air-sea interaction. Part of the momentum flux from wind transfers into the wave motion because of normal pressure force, while the other part transfers directly into the near-surface current because of friction force (Savelyev et al., 2011). It has been found that inclusion of the wind-driven current is indispensable to reproduce numerically the shift of the wave group's focusing point in the presence of wind. Although the wind-driven current is by no means uniform across the water depth, it is typical to assume in one-phase wave models a depth-uniform current profile (Touboul et al., 2006; Kharif et al., 2008; Yan and Ma, 2011; Tian and Choi, 2013).

The objective of the paper is to examine the wind effect on the evolution of a dispersive focusing wave group. As the air flow and the water waves are solved simultaneously in a single computational

domain, there is no need to introduce an empirical surface pressure model to take into account of the wind forcing effect. The wind-driven current effect could also be captured due to the wind shear generated at the air-water interface. In particular, the separate effect of wind-driven current varying strongly with depth is examined.

METHODOLOGY

Governing Equations

The governing equations for an incompressible two-phase flow can be derived by applying a convolution filter to the unsteady Navier-Stokes equations. The resulting mass continuity and momentum equations read

$$\nabla \cdot \mathbf{U} = 0 \tag{1}$$

$$\frac{\partial \rho \mathbf{U}}{\partial t} + \nabla \cdot (\rho \mathbf{U}\mathbf{U}) - \nabla \cdot (\mu_{eff} \nabla \mathbf{U}) = -\nabla p^* - \mathbf{g} \cdot \mathbf{X} \nabla \rho + \nabla \mathbf{U} \cdot \nabla \mu_{eff} \tag{2}$$

where $\mathbf{U}$ is the velocity vector, ρ is the density, p^* is the pseudo-dynamic pressure, $\mathbf{g}$ is the acceleration due to gravity, $\mathbf{X}$ is the position vector, $\mu_{eff} = \mu + \rho \upsilon_t$ is the effective dynamic viscosity, which takes into account of molecular dynamic viscosity μ and the turbulent eddy viscosity υ_t. The standard Smagorinsky model is used as the subgrid-scale model (Smagorinsky, 1963). The turbulent eddy viscosity is defined as

$$\upsilon_t = (C_s \Delta)^2 |S| \tag{3}$$

where the Smagorinsky constant $C_s = 0.167$ is used in the present study, Δ is the filter size, and $|S|$ is the magnitude of the strain rate tensor.

The two immiscible fluids of air and water are considered as one effective fluid and solved simultaneously throughout the domain. The volume fraction α acts as an indicator function to mark the location of the interface: $\alpha = 1$ if the cell is full of water, $\alpha = 0$ if the cell is full of air, and $0 < \alpha < 1$ if the cell is a mixture of the two fluids. The indicator function is tracked by the advection equation

$$\frac{\partial \alpha}{\partial t} + \nabla \cdot (\mathbf{U}\alpha) + \nabla \cdot [\mathbf{U}_c \alpha (1-\alpha)] = 0 \tag{4}$$

where an extra compression term is added to the classic VOF transport equation (Hirt and Nichols, 1985) to limit the smearing of the interface. More details about the VOF method can be found in Rusche (2002).

Numerical Methods

Eqs. 1~4 complete the mathematical description of the two-phase flow problem and are solved using a finite volume discretization and the PISO (Pressure Implicit with Splitting of Operators) algorithm. The readers are referred to Jasak (1996) for detailed description. An extended version of the OpenFOAM® based two-phase flow solver, waves2Foam (Jacobsen et al., 2012), is adopted in this study to investigate the wind-wave interaction problem. The new flow solver includes water wave generation and absorption using the relaxation zone technique.

Model Setup

Fig. 1 presents a sketch of the numerical flume, which starts from the first wave gauge station (G1) where surface elevation is available from the measurements, and extends to the right end of the physical tank (Tian and Choi, 2013). The computational domain is about 12 m long and 0.99 m high including both air and water. The minimum grid size is 2.5 mm around the interface, which is adequate based on the grid convergence study shown in the results section. The time step is automatically adjusted based on the maximum Courant number limit of 0.25.

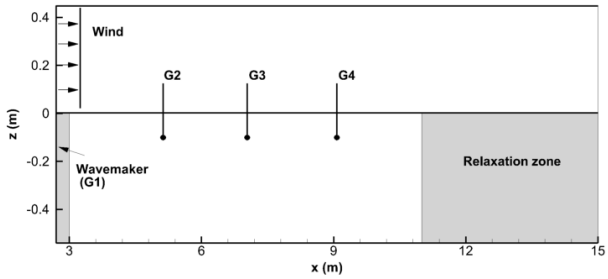

Fig. 1 Schematic of the 2D numerical wind-wave flume

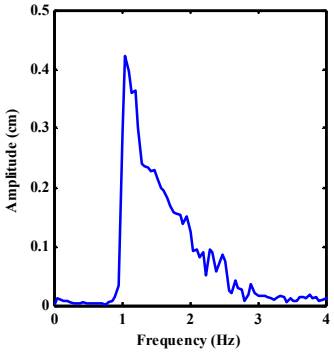

Fig. 2 Amplitude spectrum of the surface elevations measured at wave gauge G1.

The wave group generated at the physical wavemaker has a frequency band ranging from 1.0 to 2.4 Hz, peak frequency of 1.1 Hz, and initial wave steepness $\varepsilon = Na_n k_n$ equal to 0.57. The surface elevation measured at wave gauge G1 is used to drive the numerical model. The time history of surface elevation at inlet is calculated using a superposition of N = 128 linear wave components,

$$\eta(x,t) = \sum_{n=1}^{N} a_n \cos[\omega_n t - k_n (x - x_m) + \varepsilon_n] \tag{5}$$

where η is the surface elevation, the n^{th} wave component has amplitude a_n, radian frequency ω_n, wave number k_n, and phase shift ε_n, x_m is the position of the first wave gauge. The water particle velocities at the inlet are specified using the superposition of linear wave theory as well. In the presence of current with a profile, $U_c(z)$, a superposition of the wave and the current velocity is specified

$$u(x,z,t) = u_w(x,z,t) + U_c(z) \tag{6}$$

To simulate the wind effects, the numerical wind-wave flume is initialized with a steady uniform wind profile for the air, and zero velocity for the water. Since the wave height is very small in the first 10 s or so of the wave group, the wind-driven current has sufficient time to develop. To examine separately the wind-driven current effect, the velocity in the water is initialized with a steady current field, be it depth-uniform or exponentially sheared within a thin layer below the water surface. Readers are referred to Chen and Zou (2015) for the detailed setup on wave-current interaction.

RESULTS AND DISCUSSIONS

In this section, the predictions of the numerical wind-wave flume are validated against the experiment in the absence of wind and in the presence of following wind (Tian and Choi, 2013). We then examine the wind effects on the maximum surface elevations, the focusing location and the focusing time. The opposing wind effect is also studied. The separate wind-driven current effect is examined through the comparison of a depth-uniform current and an exponentially sheared surface layer current.

Grid convergence study

Fig. 3 shows the grid convergence study for a breaking wave group without wind and with following wind U_0 = 5.0 m/s. As expected, fine grid results in better agreement with the experimental data, especially for wave gauge G4 downstream the main breaking region between gauges G2 and G3. As the computational time increases significantly with finer grids, e.g. 41 h for medium grid 2.5 mm vs. 212 h for fine grid 1.25 mm on 4 cores (3.4 GHz, Fig. 3a), the medium grid was used in the following simulations.

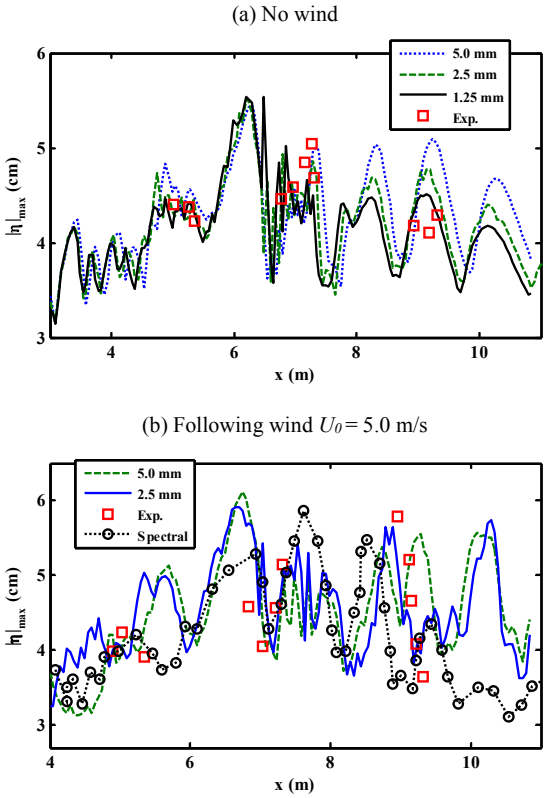

Fig. 3 Spatial distribution of maximum surface elevations (a) without wind and (b) under following wind U_0 = 5.0 m/s. Squares: experiment; dotted line with circles: pseudo-spectral model by Tian and Choi (2013).

Wave group evolution without wind

Fig. 4 presents the comparison of surface elevation history at 3 gauges (G2-G4) between present model prediction, experiment and previous pseudo-spectral model results by Tian and Choi (2013). It's seen that excellent agreement is obtained. All wave components are released simultaneously at gauge G1, with their phases adjusted so that, at some instant in time, the individual wave components are brought into focus at one spatial location. Constructive interference occurs and a large wave crest results. The focus point, defined as where the largest wave crest occurs, is located between gauges G2 and G3 for this wave group, where an active plunging breaker appears.

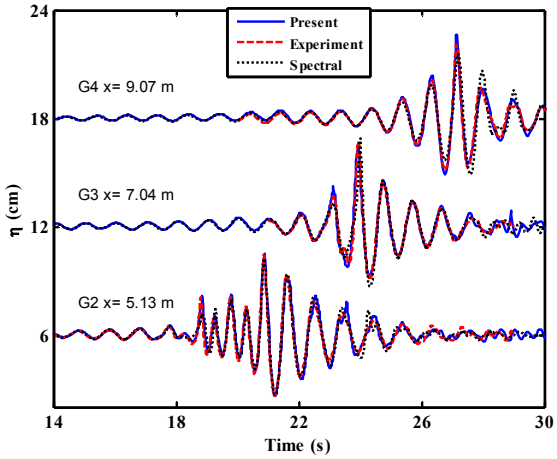

Fig. 4 Surface elevation history at 3 gauges (G2-G4) without wind. Solid line: present two-phase model; dashed and dotted lines: experiment and single-phase pseudo-spectral model by Tian and Choi (2013).

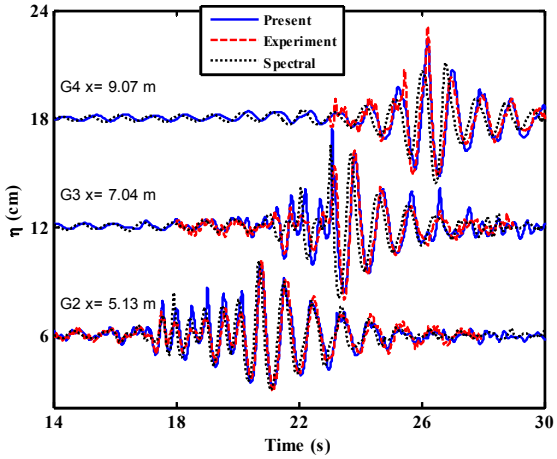

Fig. 5 Surface elevation history at 3 gauges (G2-G4) with following wind U_0 = 5.0 m/s. Solid line: present two-phase model; dashed and dotted lines: experiment and single-phase pseudo-spectral model by Tian and Choi (2013).

Wave group evolution with wind

As in the experiment, a number of following wind speeds is first considered. For the largest wind speed U_0 = 5.0 m/s, Fig. 5 presents the comparison of surface elevation history between present model prediction, experiment and previous pseudo-spectral model results by Tian and Choi (2013). It's worth noting that the present model is a two-phase flow model considering both air flow and water wave, while the pseudo-spectral model is a single-phase model considering only the water wave with the surface pressure specified by the combined Miles

and Jeffrey's model. Thus no empirical coefficients are involved in the present model. It's seen that downstream the flume, both the present model and the spectral model fail to predict the wind-generated waves observed in the experiment, which can be identified by the high frequency wave components. Compared with the spectral model, we note that the present model leads to a better phase agreement with the experimental data.

Fig. 6a presents the wind effects on the spatial distribution of maximum surface elevations under different wind speeds, while Figs. 6b~6c present the corresponding wave profiles at the focusing time and the surface elevation history at the focusing point. The positive wind speeds indicate following wind, and the negative wind speed indicates opposing wind, which blows in the opposite direction to the wave group's propagation.

Compared with the case without wind, it's demonstrated that the following wind shifts the focus point downstream, from 6.19 m without wind to 6.54 m under following wind U_0 = 3.2 m/s. Under opposing wind U_0 = -3.2 m/s, the focus point is shifted slightly upstream to 6.09 m. In correspondence to the shift of focusing point, the wave group's focusing process is delayed under following wind and expedited very slightly under opposing wind. This indicates that for this breaking wave group, the nonlinear dispersive wave group hydrodynamics is more dominant over the wind forcing and drift current under the opposing wind than under the following wind.

(a) Spatial distribution of maximum surface elevations

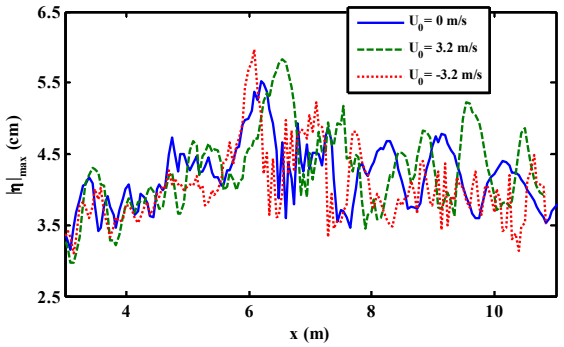

(b) Wave profiles at focusing time

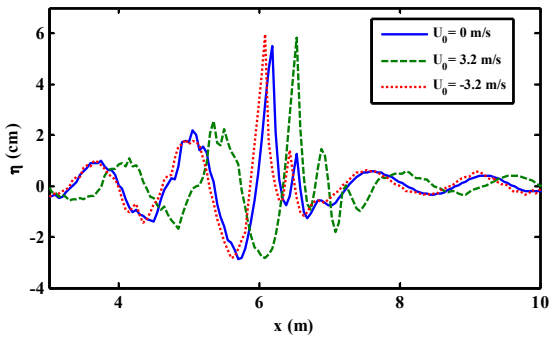

(c) Time history of surface elevation at focusing point

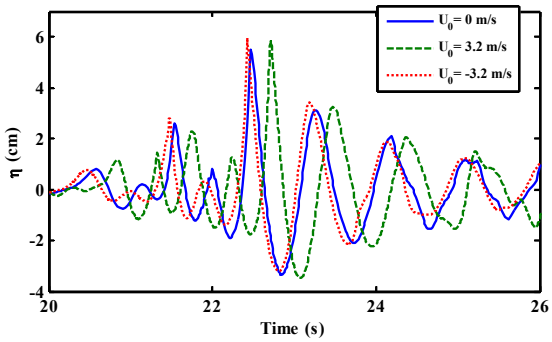

Fig. 6 Following (U_0 = 3.2 m/s) and opposing (U_0 = -3.2 m/s) wind effects on (a) the spatial distribution of maximum surface elevations, (b) wave profile at focusing time, and (c) surface elevation history at the focusing point.

Wind-driven current effect

While the wind-driven current profile in reality varies strongly with depth, it's common practice in previous investigations to use a depth-uniform current to represent the drift current effect on the wave group's evolution. The separate current effect under the largest wind forcing U_0=5.0 m/s is examined by using both a depth-uniform and an exponential layer current profile. The magnitude of the uniform current is 0.9% of the free-stream wind speed U_0, the same value as used by Tian and Choi (2013). The exponential layer current profile is of the form $U_c(z) = U_s \exp(z/\delta)$, where U_s is the surface current velocity, z is vertical coordinate, and δ is a characteristic current depth. Note that the exponential layer current decays very fast and exists only within a thin layer of about 4 cm for δ=1 cm, which is used in following simulations. The magnitude of the surface current velocity is related with the wind friction velocity, u^*, by U_s = 0.55 u^* (Wu, 1975).

Fig. 7 shows the uniform and exponential layer wind-driven current effects on the spatial distribution of maximum surface elevations. It's seen that both the depth-uniform and exponential layer current could shift the focusing point downstream as far as when both wind forcing and drift current act simultaneously.

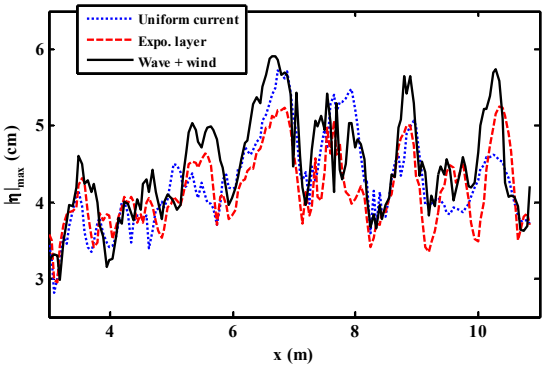

Fig. 7 Effects of uniform and exponential layer wind-driven current on the spatial distribution of maximum surface elevations. Dotted: wave + uniform current; dashed: wave + exponential layer current; solid: wave + following wind U_0 = 5.0 m/s.

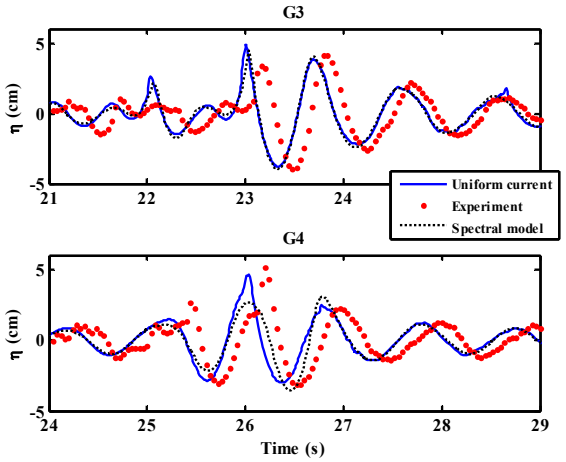

Fig. 8 Uniform current effect on the surface elevations in the presence of following wind U_0 = 5.0 m/s. Dotted line: pseudo-spectral model by Tian and Choi (2013).

Fig. 8 shows the uniform current effects on the surface elevations in the presence of following wind U_0 = 5.0 m/s. The magnitude of the depth-uniform current is 0.9% U_0, the same value as used in the pseudo-spectral model by Tian and Choi (2013). It's seen that although the uniform current is capable of shifting the focusing point downstream, it leads to phase differences in the surface elevation when compared with the experimental data. Since both the present model and the pseudo-spectral model use the same depth-uniform current to represent the wind-driven current effect, there are very good phase comparisons between the predicted surface elevations.

The exponentially sheared surface layer current is more representative of typical wind-driven current profiles than the depth-uniform currents. Fig. 9 shows the exponential layer current effect on the surface elevations. In contrast with the uniform current, the exponential layer current not only predicts the shift of focus point, but leads to better phase agreement with the experimental data. It can also be noted in Figs. 8~9 that the wind-driven current is mainly responsible for the shift of the focus point, while the direct wind forcing serves only to slightly increase the wave height.

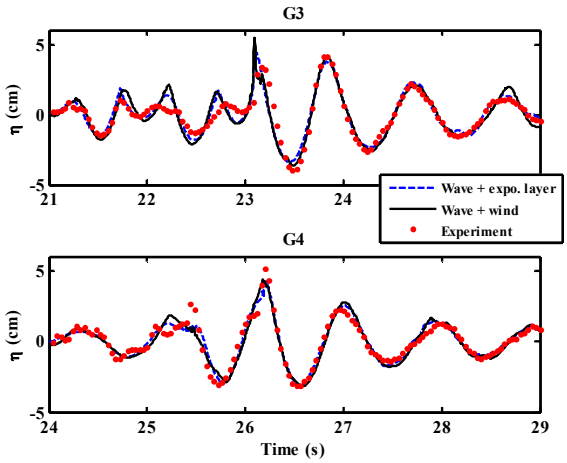

Fig. 9 Exponential layer current effect on the surface elevations in the presence of following wind U_0 = 5.0 m/s.

CONCLUSIONS

In this paper the wind effects on the evolution of a 2D dispersive focusing wave group are investigated using a two-phase flow model. As the model solves for the air flow and the waves in a single computational domain, there is no need to introduce an empirical surface pressure model to take into account of the wind forcing effect. The model predictions have been validated against the experimental data without and with following wind action. The opposing wind effect has also been considered. It's shown that the following wind delays the wave group's focusing process and shifts the focusing point downstream, while the opposing wind only slightly speeds up the focusing process and shifts the focus point upstream. The wind-driven current is mainly responsible for the shift of focusing point. While both the depth-uniform and exponential surface layer current could cause the same shift of the focusing point, the latter leads to better agreement with the experimental data.

ACKNOWLEDGEMENTS

The authors would like to thank Dr. Zhigang Tian for generously providing his experimental data and for the support of the Physical Oceanography Program of National Science Foundation under Award Numbers 1436642.

REFERENCES

Chen, Q, Kaihatu, JM, and Hwang, PA (2004). "Incorporation of wind effects into Boussinesq wave models," *J Waterway Port Coastal and Ocean Eng.*, 130(6), 312-321.

Chen, H.F., and Zou Q.P. (2015). "Numerical simulation of nonlinear wave interaction with linearly sheared currents," *Proc 25th Int Offshore and Polar Eng Conf*, Hawaii, ISOPE, 3, 538-542.

Fulgosi, M, Lakehal, D, Banerjee, S, and De Angelis, V (2003). "Direct numerical simulation of turbulence in a sheared air-water flow with a deformable interface," *J Fluid Mech.*, 482, 319-345.

Hirt, CW and Nichols, BD (1981). "Volume of fluid (VOF) method for dynamics of free boundaries," *J. Comput. Phys.* 39, 201-225.

Jacobsen, NG, Fuhrman, DR, and Fredsøe, J (2012). "A wave generation toolbox for the open-source CFD library: OpenFoam®," *Int. J. Numer. Meth. Fluids*, 70, 1073-1088. doi: 10.1002/fld.2726

Jasak, H (1996). Error analysis and estimation for the finite volume method with applications to fluid flows. Ph.D. thesis, Imperial College of Science, Technology and Medicine.

Jeffreys, H (1925). "On the formation of water waves by wind," *Proc Roy Soc London Ser A*, 189-206.

Kharif, C, and Pelinovsky, E (2003). "Physical mechanisms of the rogue wave phenomenon," *Eur J Mech B Fluids,* 22(6), 603-634.

Kharif, C, Giovanangeli, JP, Touboul, J, Grare, L, and Pelinovsky, E (2008). "Influence of wind on extreme wave events: experimental and numerical approaches," *J Fluid Mech.*, 594, 209-247.

Liu, K, Chen, Q, and Kaihatu, JM (2015). "Modeling Wind Effects on Shallow Water Waves," *J Waterway Port Coastal and Ocean Eng.*, 04015012.

Lv, X., Q.-P. Zou, Y. Zhao & D. E. Reeve 2010: "A Novel Coupled Level Set and Volume of Fluid Method for Sharp Interface Capturing on 3D Tetrahedral Grids", Journal of Computational Physics, Vol 229, Issue 7, Pages 2573-2604, (doi:10.1016/j.jcp.2009.12.005).

Miles, JW (1957). "On the generation of surface waves by shear flows," *J Fluid Mech.*, 3(02), 185-204.

Rusche, H (2002). Computational fluid dynamics of dispersed two-phase flows at high phase fractions. PhD thesis, Imperial College.

Savelyev, IB, Haus, BK, and Donelan, MA (2011). "Experimental study

on wind-wave momentum flux in strongly forced conditions," *J Phys. Oceanogr.*, 41(7), 1328-1344.
Sethian, JA, and Smereka, P (2003). "Level set methods for fluid interfaces," *Annu. Rev. Fluid Mech.*, 35(1), 341-372.
Smagorinsky, J (1963). "General circulation experiments with the primitive equations: I the basic experiment," *Mon. Weather Rev.*, 91(3), 99-164.
Sussman, M., E.G. Puckett (2000), A coupled level set and volume-of-fluid method for computing 3D and axisymmetric incompressible two-phase flows, J. Comput. Phys. 162 (2) 301–337.
Tian, Z, and Choi, W (2013). "Evolution of deep-water waves under wind forcing and wave breaking effects: numerical simulations and experimental assessment," *Eur J Mech B Fluids,* 41, 11-22.
Touboul, J, Giovanangeli, JP, Kharif, C, and Pelinovsky, E (2006). "Freak waves under the action of wind: experiments and simulations," *Eur J Mech B Fluids,* 25(5), 662-676.
Wang, Z, Zou, Q.P., and Reeve, D (2009). "Simulation of spilling breaking waves using a two phase flow CFD model," *Comput. Fluids*, 38(10), 1995-2005.
Wen X, and Mobbs S (2014). "Numerical simulations of laminar air-water flow of a non-linear progressive wave at low wind speed," *Bound.-Lay. Meteorol.*, 150, 381-398
Wu, J (1975). "Wind-induced drift currents," *J Fluid Mech.*, 68(01), 49-70.
Xie, Z (2014). "Numerical modelling of wind effects on breaking solitary waves," *Eur J Mech B Fluids,* 43, 135-147.
Yan, S, and Ma, QW (2010). "Numerical simulation of interaction between wind and 2D freak waves," *Eur J Mech B Fluids,* 29(1), 18-31.
Yan, S, and Ma, QW (2011). "Improved model for air pressure due to wind on 2D freak waves in finite depth," *Eur J Mech B Fluids,* 30(1), 1-11.
Yang, D, and Shen, L (2011). "Simulation of viscous flows with undulatory boundaries: Part II. Coupling with other solvers for two-fluid computations," *J Comp Phys.,* 230(14), 5510-5531.
Zhang, Y, Zou, Q.P., and Greaves, D (2010). "Numerical simulation of free-surface flow using the level-set method with global mass correction," *Int. J. Numer. Meth. Fluids,* 63(6), 651-680.